Second harmonic generation in gallium phosphide microdisks on silicon: from strict $\bar{4}$ to random quasi-phase matching

Pierre Guillemé, Yannick Dumeige, Julien Stodolna, Maxime Vallet, Tony Rohel, Antoine Létoublon, Charles Cornet, Anne Ponchet, Olivier Durand, Yoan Léger

Second harmonic generation in gallium phosphide microdisks on silicon: from strict $\bar{4}$ to random quasi-phase matching.

P Guillemé[1],Y Dumeige[1], J Stodolna[2], M Vallet[2], T Rohel[1], A Létoublon[1], C. Cornet[1], A Ponchet[2], O Durand[1], Y Léger[1]

[1] UMR FOTON, CNRS, INSA Rennes, Université de Rennes 1, Enssat, F35708, Rennes, France

[2] CEMES-CNRS, Université de Toulouse, UPS, 29 rue Jeanne Marvig, BP 94347 Toulouse Cedex 04, France

E-mail: yoan.leger@insa-rennes.fr

Abstract. The convergence of nonlinear optical devices and silicon photonics is a key milestone for the practical development of photonic integrated circuits. The associated technological issues often stem from material incompatibility. This is the case of second order nonlinear processes in monolithically integrated III-V semiconductor devices on silicon, where structural defects called antiphase domains strongly impact the optical properties of the material. We theoretically investigate the influence of antiphase domains on second harmonic generation in III-V whispering gallery mode microresonators on silicon and focus on the effects of the antiphase domains' mean size (i.e. the correlation length of the distribution). We demonstrate that the domain distributions can have opposite effects depending on the nonlinear process under consideration: While antiphase domains negatively impact second harmonic generation under $\bar{4}$ quasi-phase matching conditions independently of the correlation length, large conversion efficiencies can arise far from $\bar{4}$-quasi-phase matching provided that the APD correlation length remains within an appropriate range, still compatible with the spontaneous emergence of such defects in usual III-V on Si epilayers. Such a build-up can be explained by the occurrence of random quasi-phase matching in the system.

1. Introduction

Second order non-linear optics is a strategic technology for the integration of advanced photonic functions [1] and the development of non-classical light sources for applications in quantum optics [2]. In the recent years, thanks to the strong field confinement into whispering gallery modes (WGM), microring and microdisk resonators proved to be an efficient geometry to achieve frequency conversion in a large panel of materials, from $LiNbO_3$[3, 4, 5, 6, 7, 8] to III-V semiconductors [9, 10].

Among these different materials, crystals displaying a $\bar{4}$ symmetry are particularly suitable to the occurrence of $\chi^{(2)}$ phenomena in whispering gallery mode resonators. Indeed, the associated crystal and optical cavity symmetries lead to an original quasi-phase matching (QPM) condition (so-called $\bar{4}$-QPM) on the orbital momentum of the fundamental and harmonic fields [11, 12]. In the framework of second harmonic generation (SHG), the chromatic dispersion introduces a phase mismatch between the fundamental polarization and the generated second harmonic wave, leading to successive constructive and destructive interferences in the conversion process, the spatial period of which is called coherence length (Λ_{SHG}). In $\bar{4}$-crystal WGM resonators, when light turns around the [001] crystal axis, it experiences an inversion of its environment every quarter turn and thus a reversal of the macroscopic polarization. If the quarter turn distance equals the SHG coherence length, this natural polarization reversal precisely compensates the phase mismatch between the fundamental and the second harmonic and large conversion efficiencies can be obtained. First promising experimental results were recently obtained in monolithic GaAs [9], AlGaAs [13] and GaP microdisks [14].

The integration of such devices on silicon photonic platforms still remains challenging [10, 15] but is particularly relevant with GaP thanks to its quasi-lattice matching with Si. The heteroepitaxial growth of III-V compounds on Si has been studied for years [16, 17], and a taxonomy of integration-induced defects has been established [18]. Among them, antiphase domains (APDs) are of prime importance as far as second order nonlinearity is concerned in future Si-integrated devices. APDs, initiated at the III-V/Si interface, consist in local inversions of III and V atoms in the crystal lattice due to the growth of a polar material on a non-polar one [19]. They thus induce a spatial distribution of opposite nonlinear susceptibility domains in the material. When such a distribution is tailored into a periodical arrangement, at the cost of complicated fabrication steps, APDs can be beneficial to SHG as demonstrated in orientation-patterned GaAs/Ge waveguides [20]. But, most of the time, the spontaneous appearance of APDs leads to random spatial distributions that lowers the efficiency of the nonlinear process [21]. In a previous work we notably demonstrated that APDs could be used to cancel the nonlinear conversion in a specific region of the disk in order to unlock novel modal QPM schemes in WGM resonators [22].

Conversely, in this work, we theoretically investigate the conditions where random APD distributions in GaP microdisks monolithically integrated on silicon, instead of canceling SHG, directly benefit to the nonlinear process. Two cases must be

distinguished: When fundamental and second harmonic modes satisfy the $\bar{4}$-QPM condition, occurrence of APDs in the system can only reduce the overall conversion efficiency of the nonlinear process. On the contrary, far from any $\bar{4}$-QPM condition, ADPs can enable random quasi-phase matching between two resonant modes [23]. The predicted conversion efficiencies obtained in this way remain significant as long as the APD correlation length lays within a specific but realistic range. Our consideration of APDs is based on the treatment of plan-view dark field transmission electron microscopy (TEM) measurements, allowing us to extract both the mean polarity and the correlation length of real APD distributions. A large number of numerically generated realistic APDs is then introduced in our SHG simulations to statistically infer the relative impact of each parameter on the nonlinear conversion efficiency for each case of SHG.

2. Methods

In defect-free GaP microdisks, the SHG efficiency can be analytically estimated [24]. The Helmholtz equation describing the propagation of the optical waves in the microdisk is solved by variable separation for both fundamental (f) and second harmonic (SH) modes. In the following, $\tilde{Z}(z)$ is the normalized dependence of the field along the disk axis and $\tilde{\psi}(r)$, the radial normalized one. The azimuthal dependence is harmonic with m_f and m_{SH}, the azimuthal numbers for the fundamental and the second harmonic respectively. We note $\Delta m = m_{SH} - 2m_f$ the orbital momentum mismatch during the nonlinear process. Only the modes fulfilling the conditions for an efficient SHG, in particular modes that are doubly resonant in the microdisk, are selected. In this framework, the overlap between the fundamental and the SH WGM reads [24]:

$$\tilde{K}_{\pm} = \frac{\mp 1}{2\epsilon_0 \omega_{SH} n_f^4} \int_{-h/2}^{h/2} \tilde{Z}_{SH} \tilde{Z}_f^2 \int_0^R \int_0^{2\pi} d_{14}(\mathbf{r}) \times e^{i(\Delta m \pm 2)\theta} r \tilde{\psi}_{SH} \left(\frac{m_f}{r} \tilde{\psi}_f \pm \frac{d\tilde{\psi}_f}{dr} \right)^2 dr d\theta dz \quad (1)$$

where d_{14} is the relevant element of the nonlinear-susceptibility-tensor in $\bar{4}3m$ crystals, the spatial dependence of which will be discussed later on, n_f the refractive index at the fundamental mode wavelength, h and R, the thickness and the radius of the microdisk.

Finally, the coupling of the light into the microdisk thanks to evanescent propagating modes through tapered optical fibers is taken into account and leads to the following expression:

$$\eta = P_{in} |\tilde{K}_- + \tilde{K}_+|^2 \times \frac{\alpha_{SH}^2 (1 - |t_{SH}|^2)}{(1 - \alpha_{SH}|t_{SH}|)^2} \times \left[\frac{\alpha_f^2 (1 - |t_f|^2)}{(1 - \alpha_f |t_f|)^2} \right]^2 \quad (2)$$

where P_{in} is the power of the fundamental, $\alpha_{f(SH)}$ the sum of the scattering and radiation losses in the microdisk for the fundamental (SH) mode, $t_{f(SH)}$ the transmission of the

taper for the fundamental (SH) mode. These last values can be calculated from the intrinsic (Q^{int}) and the coupling (Q^{cpl}) quality factor respectively [25]:

$$Q = \pi m \frac{\sqrt{x}}{1-x} \tag{3}$$

where x is replaced by α for the intrinsic quality factor and $|t|$ for the coupling quality factor.

In the following, we first consider a GaP microdisk of thickness $h = 150$ nm and radius $R = 2.503$ μm which lets a QPM between two resonant modes with unitary radial and planar numbers such as $\lambda_f = 1697$ nm. Assuming an homogeneous nonlinear susceptibility [26] $d_{14} = 28.5$ pm.V^{-1} and an overall quality factor of 5.10^3 with $Q^{int} = Q^{cpl}$, we find a SHG efficiency of 1.1 %.mW^{-1} in a single-phase microdisk. We will first focus on the effect of APDs on the nonlinear process involving these two modes in the QPM configuration and in a second part we will analyze the impact of APDs on nonlinear processes far from this condition.

The appearance of APDs in the GaP microdisk is expected to affect strongly this conversion efficiency. The crystal polarity $P_{APD}(\mathbf{r})$ must then be defined locally, taking the values ± 1 depending on the atomic ordering at position $\mathbf{r}$. This local definition of the crystal polarity allows us to describe the spatial evolution of the nonlinear susceptibility, $d_{14}(\mathbf{r}) = P_{APD}(\mathbf{r})|d_{14}|$, to be introduced in Eq.(1). In the following, we will restrict the study to the case where APDs are invariant along z, which generally happens when no particular method is used to annihilate them during the III-V growth [27].

The planar distribution of APDs can be investigated through dark field transmission electron microscopy on the $g = (002)$ diffraction peak, which intensity strongly depends on local polarity inversions [28]. Figure 1(a) shows such a large scale TEM plan view of a typical 20 nm thick GaP epilayer grown by migration enhanced epitaxy on a 4°-off vicinal [001] Si substrate. Antiphase domains with opposite polarities appear as light and dark gray areas. Maintaining a good contrast between APDs over such a large field of view (300×180 nm) is particularly challenging as the TEM intensity also depends on other factors like lateral fluctuations of the sample thickness [28]. If these images are too small to be directly used in SHG simulations (a disk area is 370 times larger), they are however sufficient to statistically measure the parameters of APD distributions. To do so, we first apply a threshold mask to figure 1(a) to separate the APDs into ± 1 areas. The mean sample polarity is then obtained by averaging the thresholded image of the polarity distribution $d_{14}(\mathbf{r})$ presented in figure 1(b) and the APD correlation length is extracted from the HWHM of the lorentzian profile of minority domains in the Fourier transform $\mathcal{F}(d_{14}(\mathbf{r}))(\mathbf{k})$ presented in figure 2 (a) and (b). The sample presented here features a mean polarity $\langle P_{APD} \rangle = 0.5 \pm 0.1$, the accuracy of which is limited by the resolution of the TEM image analysis method; the APD distribution is slightly anisotropic as observed in figure 2 (a), with correlation lengths L_c of 8 and 12 nm along the main anisotropy axes (with accuracy of ± 2 nm).

In order to investigate the effects of APDs on SHG in semiconductor microdisks on silicon, we thus compute artificial APD distributions with 25 μm^2 areas. The used

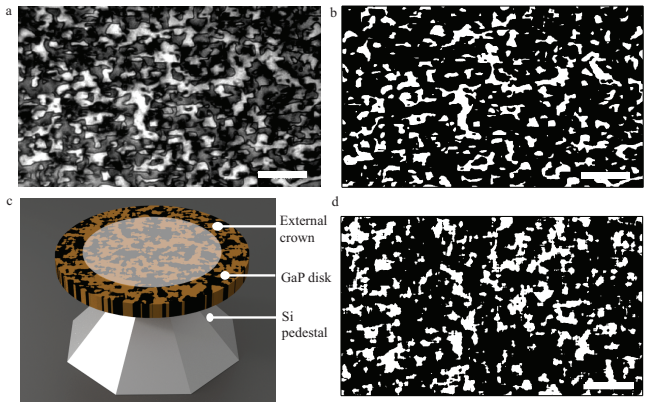

Figure 1. **a.** Plan-view TEM micrograph in (002) dark field conditions of a 20 nm-thick GaP/Si sample grown by molecular beam epitaxy. **b.** Thresholded pattern deduced from a. **c.** Sketch of a GaP microdisk featuring APDs on a Si pedestal, and the 20 % external crown. **d.** Artificial picture made from a mathematical Fourier modelization. The white bar is 50 nm long on all graphs.

procedure was first developed to mimic thresholded distributions obtained from real patterns as shown in figure 1(b) and (d) and then applied to the generation of APD distributions of arbitrary mean polarity, APD correlation length L_c and APD anisotropy. To do so, a k-space pattern with 0.2 μm^{-1} resolution and 400 μm^{-1} span is calculated with white noise phase and amplitude distributions. Lorentzian amplitude envelopes along the main crystal axes are imposed to fix the APD correlation length in k-space as shown in figure 2(c). Reverse Fourier transform and thresholding is then used to obtain real space APD distributions similar to the one of figure 1(d). They are finally converted into sign distributions for d_{14} to calculate Eq. (1). For each artificial APD distribution, we finally recalculate $\langle P_{APD} \rangle$ and L_c as the final thresholding step can introduce a small mismatch with the targeted values. Actually, since the WGM are located on the periphery, the overlap between the fundamental and the SH is different from zero only on the 20 % external part of the microdisk. Thus, the mean polarity $\langle P_{APD} \rangle$ is calculated only on the external crown represented in figure 1(c).

3. Results

Using the same geometrical and QPM conditions as for the single phase GaP SHG discussed above, the SHG conversion efficiency for 1 mW of incident fundamental power is calculated for a large set of artificial APD realizations and plotted as a function of the external crown mean polarity $\langle P_{APD} \rangle$ and correlation length Lc on figure 3 and figure 4 respectively.

Figure 3 shows a quadratic dependence of the conversion efficiency that can be intuited through the analysis of equations (1) and (2) if the APD distribution is uncorrelated with the mode profiles. This dependence leads to a severe decrease of the conversion efficiency when $\langle P_{APD} \rangle$ is progressively decreased to 0. Typically, when

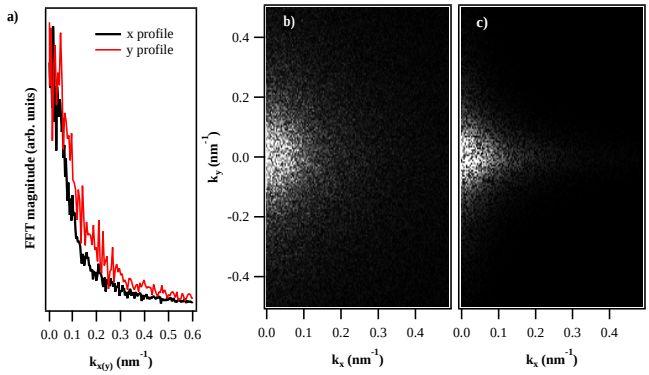

Figure 2. Spatial Fourier transforms of the experimental (**b.**) and theoretical (**c.**) APD distributions presented in figures 1(b) and (d) respectively. **a.** Profiles of the experimental APD Fourier transform along the x and y directions, unveiling a slight anisotropy.

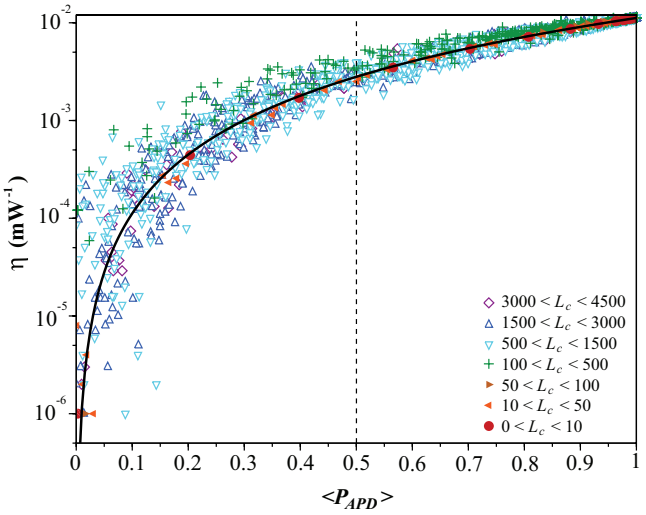

Figure 3. Calculated SHG efficiency in microdisks with artificial APD distributions for 1 mW of fundamental power as a function of $\langle P_{APD} \rangle$. The maximal value of $\eta = 10^{-2}$ mW^{-1} corresponds to ideal $\bar{4}$-QPM conditions in the absence of APDs. The different colors/markers correspond to different APD correlation lengths L_c (in nm). The black curve is a parabolic fit. The dotted line indicates the mean polarity of the experimental TEM measurement of figure 1(b).

the imbalance between +1 and −1 domains is only 10% ($\langle P_{APD} \rangle = 0.1$), the conversion efficiency is two orders of magnitude smaller than the single phase case. However, realistic distributions of APDs are not necessarily balanced as shown by figure 1(a). For this experimental case where $\langle P_{APD} \rangle = 0.5 \pm 0.1$, the efficiency lowering is only of a factor 3 to 5, keeping the nonlinear process within an acceptable range.

When the correlation length of the APDs is lower than 100 nm, the calculated efficiencies follow with high accuracy the quadratic dependence (red circles and orange triangles in figure 3), while for domains with L_c larger than 1.5 μm (open blue triangles

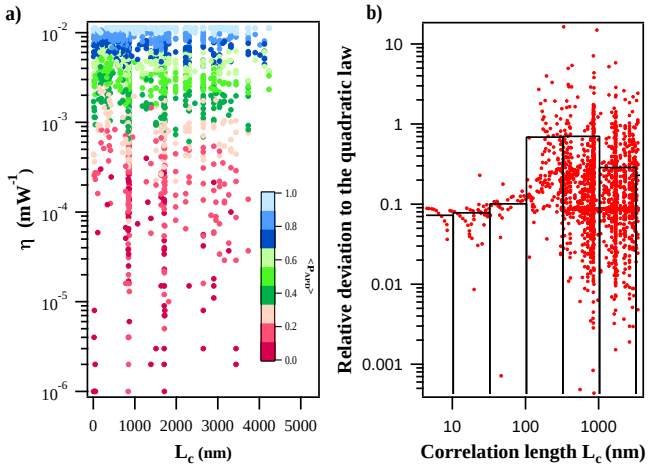

Figure 4. a) Calculated conversion efficiency η as a function of the APD correlation length L_c for different values of the mean polarity $\langle P_{APD} \rangle$. b) Relative deviations of η to the quadratic law plotted in figure 3 for each APD realization as a function of L_c (red dots). These values are used to calculate the relative standard deviation of η for different L_c ranges (black bar plot).

and purple diamonds), the standard deviation is large (this feature will be quantified further on). This shows how the finite size of the microdisk influences the conversion efficiency through the sampling of the APD distribution. For large L_c values, close to the disk radius, the APD distribution within the disk is not statistical anymore and large variations of η are observed.

The conversion efficiency of the different realizations versus the APD correlation length is presented in figure 4(a). When varying L_c from the experimentally measured values ($\sim$ 10 nm) to the coherence length Λ_{SHG} of the nonlinear process ($\sim$ 4 μm) we observe no significant evolution of the conversion efficiency at fixed mean polarity $\langle P_{APD} \rangle$ (indicated by the marker colors in figure 4). Moreover, natural APD distributions can show anisotropy as illustrated in figure 2(a). We thus also investigated the impact of APD anisotropy on the the conversion efficiency (not presented here). The variation of the APD correlation planar aspect ratio from 1 to 10 does not affect the conversion efficiency either.

Furthermore, figure 4(b) gives us information on the dispersion of the SHG conversion efficiency induced by the random nature of the APD distributions. The larger the correlation lengths of the APD distributions, the larger the dispersion on the calculated conversion efficiency. As aforementioned, the finite size of the microdisk samples the APD distribution, which becomes non-statistical as the correlation approaches the disk radius. We calculated the relative standard deviation to the quadratic law for different ranges of L_c. We observe that the dispersion of the conversion efficiency η on the different realizations remains below 10% when the correlation length is below a few hundreds of nanometers while it approaches unity for larger values of L_c. This result highlights the physical limit of the APD scale for the use of natural APD

patterns for second order nonlinear applications in such systems.

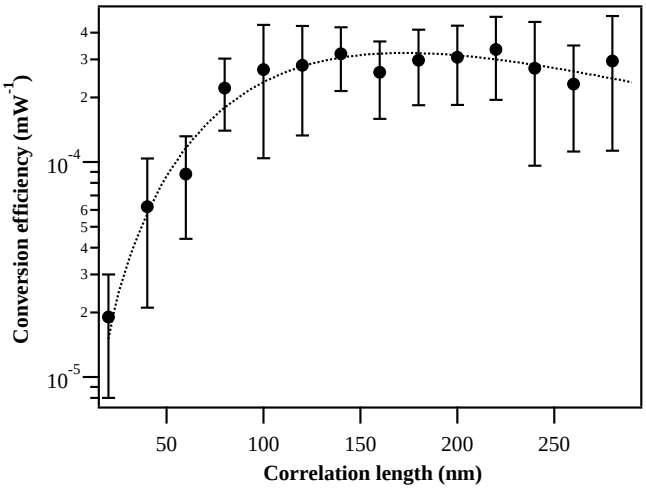

Figure 5. Dependence of the calculated conversion efficiency η on the correlation length L_c for $\langle P_{APD} \rangle = 0$ in a GaP microdisk on Si where the double resonance is obtained on modes featuring an azimuthal mismatch $\Delta m = 8$ (black circles). The error bars show the standard deviation for multiple APD distributions featuring the same L_c and P_{APD}. The dotted (dashed) curve is a fit based on (1), consisting in the square modulus of a linear combination of the two relevant Fourier components of $d_{14}(\mathbf{r})$ at spatial frequencies k_6 and k_{10}, assuming the Lorentzian profile of the Fourier space APD distribution.

So far, the microdisk geometry was tuned to address a specific $\bar{4}$-QPM condition, the efficiency of which could only be altered by the randomicity of the crystal polarity. On the contrary, if the geometrical parameters of the microdisk are now chosen to get a double resonance for two modes (f, SH) far from any $\bar{4}$-QPM condition, Random QPM can then efficiently enable SHG [23, 29]. Figure 5 shows the conversion efficiency η when the APD correlation length is varied in a microdisk where the double resonance is obtained for the modes: ($\lambda_f = 1523$ nm, $m_f = 14$) and ($\lambda_{SH} = 761.5$ nm, $m_{SH} = 36$) (requiring a disk radius $R = 2.01$ μm and thickness of 178 nm). In this case the $\bar{4}$-QPM cannot annihilate the phase term in (1) since $\Delta m = 8$ but specific spatial frequency components of $d_{14}(\mathbf{r})$ can. In figure 5 a build-up of the conversion efficiency is clearly observed. This evolution of η is successfully fitted by the square modulus of a linear combination of the two relevant Fourier components of $d_{14}(\mathbf{r})$: namely $\mathcal{F}(d_{14}(\mathbf{r}))(k_6)$ and $\mathcal{F}(d_{14}(\mathbf{r}))(k_{10})$ where $k_6 = 0.48$ μm^{-1} and $k_{10} = 0.8$ μm^{-1} are the ad-hoc spatial frequencies which compensate the total azimuthal mismatch $\Delta m \pm 2$ (dotted line in figure 5). These Fourier components follow a Lorentzian law according to our generation process of the APDs. From equation (2) the conversion efficiency can thus be written as:

$$\eta \propto \left| \frac{O_+ L_c}{1 + (k_6 L_c)^2} + \frac{O_- L_c}{1 + (k_{10} L_c)^2} \right|^2 \tag{4}$$

where O_+ and O_- take into account the field overlap given by equation (1) and the

double resonance enhancement.

4. Discussion

To assess the interest of such a random QPM process in microdisks compared to other SHG schemes, three features should be discussed: the conversion efficiency, the wavelength conversion window and the tolerance of the device to fabrication dispersion. Figure 6 a) summarizes the conversion efficiencies η of four SHG schemes in GaP microdisks as a function of the fundamental mode wavelength: i) the ideal $\bar{4}$-QPM schemes where fundamental and SH modes share the same confinement numbers; ii) the case reported in [14] where $\bar{4}$-QPM is coupled to radial-modal-QPM; iii) the case reported in our previous work [22] where vertical-modal QPM is enabled by APDs and associated with $\bar{4}$-QPM; iv) the presently discussed random QPM scheme. For the sake of validity of such a comparison, we do not consider directly the experimental result of case ii) but its theoretical equivalent with parameters matching those of the present simulations in terms of Q factors. The geometrical parameters of the disks are also provided in figure 6.
If the conversion efficiency of the random QPM scheme remains in the best case one order of magnitude below the ideal case of $\bar{4}$-QPM, it is clearly competitive compared to other SHG schemes, especially the only experimentally reported case in GaP-microdisks (case iii). This is verified even if the APD correlation length is not optimized ($L_c \sim 50$ nm) and close to reported experimental values.

Still, the sole discussion on the conversion efficiency is not sufficient to legitimate random quasi-phase matching compared to the ideal $\bar{4}$-QPM and the APD-assisted scheme of Ref.[22]. For these two schemes, SHG is determined by both the double resonance condition (i.e. a WGM at twice the fundamental frequency must exist) and the strict $\bar{4}$-QPM ($\Delta m = \pm 2$). This makes the conditions to obtain SHG quite rare as revealed by figure 6 b): for the ideal SHG case, there is only a single couple (R, h) of the disk radius and disk thickness which makes SHG possible at a given wavelength and for a given fundamental azimuthal number m_f. A similar behavior is observed for all $\bar{4}$-QPM schemes (cases i), ii) and iii)). In the phase space represented in figure 6, the SHG solution ensemble is then composed of separated lines associated with the different m_f. The rarity of these SHG conditions explains the difficulty to observe experimentally SHG in the best configuration where fundamental and SH modes share the same radial number [9, 14]. In spite of this, in the random QPM case, only the double resonance condition remains: SHG can be found for any Δm between the fundamental and SH modes. In a specific region of the phase space, the solution ensembles for consecutive Δm overlap, greatly increasing the probability to find a (R, h) couple allowing SHG at a given wavelength. More than this, one also observes that a solution ensemble is denser for higher Δm values, which still increases this effect. Random quasi-phase matching in GaP microdisks on silicon thus offers a release of the SHG constraints in return for an acceptable decrease of the conversion efficiency. The remaining constraint, i.e.

the doubly resonant condition, can also be alleviated using thermo-optic effects due to intracavity absorption [14].

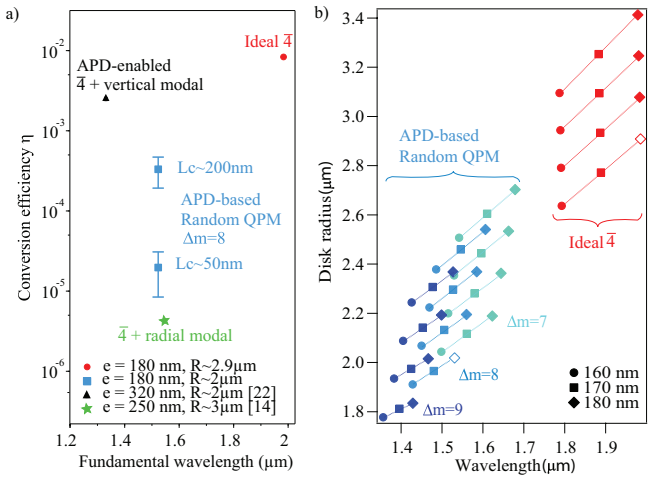

Figure 6. a) Calculated SHG conversion efficiencies for different QPM schemes as a function of the fundamental mode wavelength. b) Required disk radius as a function of the targeted wavelength and for a 20 nm thickness span around 170 nm. The two open diamonds correspond to the configurations presented in a). The different color lines show the solutions for a single azimuthal number of the fundamental mode (from the bottom line to the top line: $m_f = 14$ to 17), in each case.

High conversion efficiencies, above $10^{-4}/\mathrm{mW}^{-1}$, for both schemes can be conserved for $50 < L_c < 300$ nm, close to values theoretically obtained when double resonance is not perfectly obtained in strict $\bar{4}$-QPM schemes due to fabrication flaws [24] or when modal and $\bar{4}$-QPM are combined in GaP microdisks on Si [22]. These results highlight the broadband nature of random QPM [30], which could constitute a leading advantage in comparison to $\bar{4}$-QPM in future devices on Si. The correlation lengths required to optimize the random QPM remain in the range where sub-sampling of the APD distribution does not affect the dispersion of multiple realizations. Specific growth strategies may be used to tailor the correlation length of APDs to such values [31, 32]. Random QPM in microdisks is thus particularly attractive to free SHG from strict selection rules while preserving the nonlinear process magnification induced by optical confinement, provided that the APD correlation length can be tailored in future experiments.

5. Conclusion

In conclusion, the integration of GaP microdisks would be of great interest to realize nonlinear photonics functions on Si. While GaP demonstrated promising advantages in both nonlinear optics and silicon photonics, the convergence of these domains still appears challenging. Indeed, the heteroepitaxial growth of GaP on Si leads to the formation of APDs which have a huge impact on the nonlinear properties of photonic

devices. We demonstrated that, while the natural randomicity of APD distributions is detrimental to SHG when strict $\bar{4}$-QPM conditions are aimed for, it also unlocks new QPM conditions for other modes, with non-negligible conversion efficiencies. This opens new routes for the realization of efficient broadband nonlinear photonic devices on Si.

Acknowledgments

This research was supported by the Labex CominLabs through the "3D Optical Many Cores" project, the French National Research Agency Project ANTIPODE (Grant No. 14-CE26-0014-01), the Région Bretagne, Rennes Métropole and the Institut Universitaire de France (IUF).

References

[1] Andrea Guarino, Gorazd Poberaj, Daniele Rezzonico, Riccardo Degl'Innocenti, and Peter Günter. Electro-optically tunable microring resonators in lithium niobate. *Nature Phot.*, 1(7):407–410, July 2007.

[2] J. L. O'Brien. Optical Quantum Computing. *Science*, 318(5856):1567–1570, December 2007.

[3] J. U. Fürst, D. V. Strekalov, D. Elser, M. Lassen, U. L. Andersen, C. Marquardt, and G. Leuchs. Naturally Phase-Matched Second-Harmonic Generation in a Whispering-Gallery-Mode Resonator. *Phys. Rev. Lett.*, 104(15):153901, 2010.

[4] Cheng Wang, Michael J. Burek, Zin Lin, Haig A. Atikian, Vivek Venkataraman, I-Chun Huang, Peter Stark, and Marko Lončar. Integrated high quality factor lithium niobate microdisk resonators. *Opt. Express*, 22(25):30924, December 2014.

[5] Kiyotaka Sasagawa and Masahiro Tsuchiya. Highly efficient third harmonic generation in a periodically poled $MgO : LiNbO_3$ disk resonator. *Appl. Phys. Express*, 2(12):122401, 2009.

[6] Sarah-Katharina Meisenheimer, Josef Urban Fürst, Christoph Werner, Tobias Beckmann, Karsten Buse, and Ingo Breunig. Broadband infrared spectroscopy using optical parametric oscillation in a radially-poled whispering gallery resonator. *Opt. Express*, 23(18):24042–24047, Sep 2015.

[7] Vladimir S. Ilchenko, Anatoliy A. Savchenkov, Andrey B. Matsko, and Lute Maleki. Nonlinear optics and crystalline whispering gallery mode cavities. *Phys. Rev. Lett.*, 92:043903, Jan 2004.

[8] Jintian Lin, Yingxin Xu, Jielei Ni, Min Wang, Zhiwei Fang, Lingling Qiao, Wei Fang, and Ya Cheng. Phase-matched second-harmonic generation in an on-chip $LiNbO_3$ microresonator. *Phys. Rev. Applied*, 6:014002, Jul 2016.

[9] Paulina S. Kuo, Jorge Bravo-Abad, and Glenn S. Solomon. Second-harmonic generation using $\bar{4}$-quasi-phasematching in a GaAs whispering-gallery-mode microcavity. *Nature Comm.*, 5:3109, January 2014.

[10] Chi Xiong, Wolfram Pernice, Kevin K. Ryu, Carsten Schuck, King Y. Fong, Tomas Palacios, and Hong X. Tang. Integrated GaN photonic circuits on silicon (100) for second harmonic generation. *Opt. Express*, 19(11):10462, May 2011.

[11] Yannick Dumeige and Patrice Féron. Whispering-gallery-mode analysis of phase-matched doubly resonant second-harmonic generation. *Phys. Rev. A*, 74(6):063804, 2006.

[12] P. S. Kuo, W. Fang, and G. S. Solomon. $\bar{4}$-quasi-phase-matched interactions in GaAs microdisk cavities. *Opt. Lett.*, 34(22):3580–3582, Nov 2009.

[13] S. Mariani, A. Andronico, A. Lemaître, I. Favero, S. Ducci, and G. Leo. Second-harmonic generation in AlGaAs microdisks in the telecom range. *Opt. Lett.*, 39(10):3062, May 2014.

[14] David P. Lake, Matthew Mitchell, Harishankar Jayakumar, Las Fujii dos Santos, Davor Curic, and

Paul E. Barclay. Efficient telecom to visible wavelength conversion in doubly resonant gallium phosphide microdisks. *Appl. Phys. Lett.*, 108(3):031109, January 2016.

[15] M. M. R. Howlader, T. Suga, and M. J. Kim. Room temperature bonding of silicon and lithium niobate. *Appl. Phys. Letters*, 89(3), 2006.

[16] Herbert Kroemer. Polar-on-nonpolar epitaxy. *J. Cryst. Growth*, 81(1):193–204, 1987.

[17] Andrew Lee, Huiyun Liu, and Alwyn Seeds. Semiconductor III-V lasers monolithically grown on Si substrates. *Semicond. Sci. and Tech.*, 28(1):015027, 2013.

[18] Yan Ping Wang, Antoine Letoublon, Tra Nguyen Thanh, Mounib Bahri, Ludovic Largeau, Gilles Patriarche, Charles Cornet, Nicolas Bertru, Alain Le Corre, and Olivier Durand. Quantitative evaluation of microtwins and antiphase defects in GaP/Si nanolayers for a III-V photonics platform on silicon using a laboratory X-ray diffraction setup. *J. Appl. Crystallogr.*, 48(3):702–710, June 2015.

[19] Oliver Supplie, Sebastian Brückner, Oleksandr Romanyuk, Henning Döscher, Christian Höhn, Matthias M. May, Peter Kleinschmidt, Frank Grosse, and Thomas Hannappel. Atomic scale analysis of the GaP/Si(100) heterointerface by *in situ* reflection anisotropy spectroscopy and *ab initio* density functional theory. *Phys. Rev. B*, 90:235301, Dec 2014.

[20] Xiaojun Yu, Luigi Scaccabarozzi, Angie C. Lin, Martin M. Fejer, and James S. Harris. Growth of GaAs with orientation-patterned structures for nonlinear optics. *J. Cryst. Growth*, 301302:163–167, 2007.

[21] D. J. Bottomley, J.-M. Baribeau, and H. M. van Driel. Limitations to the realization of noncentrosymmetric Si_mGe_n superlattices. *Phys. Rev. B*, 50:8564–8568, Sep 1994.

[22] P. Guillemé, M. Vallet, J. Stodolna, A. Ponchet, C. Cornet, A. Létoublon, P. Féron, O. Durand, Y. Léger, and Y. Dumeige. Antiphase domain tailoring for combination of modal and $\bar{4}$-quasi-phase matching in gallium phosphide microdisks. *Opt. Express*, 24(13):14608–14617, Jun 2016.

[23] M. Baudrier-Raybaut, R. Haïdar, Ph. Kupecek, Ph. Lemasson, and E. Rosencher. Random quasi-phase-matching in bulk polycrystalline isotropic nonlinear materials. *Nature*, 432(7015):374–376, November 2004.

[24] Paulina S. Kuo and Glenn S. Solomon. On- and off-resonance second-harmonic generation in GaAs microdisks. *Opt. Express*, 19(18):16898, August 2011.

[25] A. Yariv. Universal relations for coupling of optical power between microresonators and dielectric waveguides. *Electron. Lett.*, 36(4):321, 2000.

[26] Ichiro Shoji, Takashi Kondo, Ayako Kitamoto, Masayuki Shirane, and Ryoichi Ito. Absolute scale of second-order nonlinear-optical coefficients. *J. Opt. Soc. Am. B*, 14(9):2268, September 1997.

[27] I. Németh, B. Kunert, W. Stolz, and K. Volz. Heteroepitaxy of GaP on Si: Correlation of morphology, anti-phase-domain structure and MOVPE growth conditions. *J. Cryst. Growth*, 310(7-9):1595–1601, 2008.

[28] Igor Németh. *Transmission electron microscopic investigations of heteroepitaxial III/V semiconductor thin layer and quantum well structure.* PhD thesis, Philipps Universität Marburg, 2008.

[29] Xavier Vidal and Jordi Martorell. Generation of light in media with a random distribution of nonlinear domains. *Phys. Rev. Lett.*, 97:013902, Jul 2006.

[30] Luis Mateos, Pablo Molina, Juan F. Galisteo-Lpez, Cefe Lpez, Luisa E. Baus, and Mariola O Ramrez. Ultrabroadband generation of multiple concurrent nonlinear coherent interactions in random quadratic media. *Applied Physics Letters*, 103(10), 2013.

[31] T. J. Grassman, M. R. Brenner, S. Rajagopalan, R. Unocic, R. Dehoff, M. Mills, H. Fraser, and S. A. Ringel. Control and elimination of nucleation-related defects in GaP/Si(001) heteroepitaxy. *Appl. Phys. Lett.*, 94(23), 2009.

[32] Kerstin Volz, Andreas Beyer, Wiebke Witte, Jens Ohlmann, Igor Németh, Bernardette Kunert, and Wolfgang Stolz. GaP-nucleation on exact Si (0 0 1) substrates for III/V device integration. *J. Cryst. Growth*, 315(1):37 – 47, 2011. 15th International Conference on Metalorganic Vapor Phase Epitaxy (ICMOVPE-XV).